Recycling of ferronickel slag tailing in cementitious materials
Activation and performance

Chi, Lin; Lu, Shuang; Li, Zhenming; Huang, Chendong; Jiang, Hui; Peng, Bin

DOI
10.1016/j.scitotenv.2022.160706

Publication date
2023

Document Version
Final published version

Published in
Science of the Total Environment

Science of the Total Environment 861 (2023) 160706

Contents lists available at ScienceDirect

Science of the Total Environment

journal homepage: www.elsevier.com/locate/scitotenv

Recycling of ferronickel slag tailing in cementitious materials: Activation and performance

Lin Chi [a], Shuang Lu [b,c,*], Zhenming Li [d], Chendong Huang [a], Hui Jiang [b,c], Bin Peng [a,**]

[a] School of Environment and Architecture, University of Shanghai for Science and Technology, Shanghai 200093, China
[b] School of Civil Engineering, Harbin Institute of Technology, Harbin 150001, China
[c] Key Lab of Structures Dynamic Behavior and Control of the Ministry of Education, Harbin Institute of Technology, Harbin 150090, China
[d] Department of Materials, Mechanics, Management & Design, Delft University of Technology, Delft, 2628 CN, the Netherlands

HIGHLIGHTS

- Recycled FNS powders can be applied as the SCMs for carbon footprint reduction.
- With the content exceeding 10 %, the insufficient pretreated FNS can hardly participate in the hydration reaction.
- The reactivity of FNS can be effectively enhanced by mechanical grinding and steam curing pretreatment.

GRAPHICAL ABSTRACT

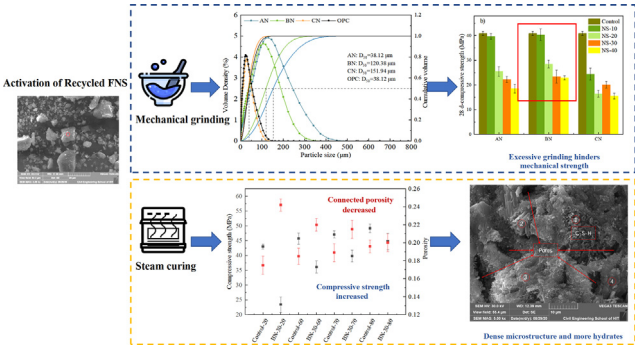

ARTICLE INFO

Editor: Daniel CW Tsang

Keywords:
Ferronickel slag
SCMs
Hydration mechanism
Grinding and heat curing

ABSTRACT

As an industrial by-product containing pozzolanic components, recycled ferronickel slag (FNS) has the potential to be supplementary cementitious materials (SCMs) to reduce the massive carbon footprint of the cement industry, however, the main limitation of ferronickel slag as SCMs is the low hydration rate at an early age. In this study, the pozzolanic activity property results indicate that if the proportion is more than 10 %, FSN can hardly participate in the cement hydration reaction during the early stage, even the mechanical strength of FNS-mortar decreases obviously with the higher proportion of ferronickel slag. Therefore, mechanical grinding and steam curing at an early age are applied to promote the reaction activity of the recycled ferronickel slag tailing in this study. Compared with standard curing, the compressive strength of hardened FNS-cement paste with steam curing at 60 °C or 80 °C increased by 8.2 % or 33.8 %, and the connected porosity decreased by 18.9 % or 17.3 %. And MgO in the ferronickel slag exists as Mg_2SiO_4 in raw materials and enters the C-S-H gel with the formation of M-S-H gel during the secondary hydration stage. This study provides a theoretical basis for solid waste-based concrete and promotes the recycling, conservation, and resources of solid waste in building materials.

1. Introduction

Cement production is considered as one of the massive carbon-polluting industries. In recent years, cement industry is suggested to apply a combination of waste-based alternatives and carbon capture/storage technology to reduce CO_2 emissions (Gartner and Hirao, 2015; Kaliyavaradhan et al., 2020; Shi and Wu, 2008). Industrial by-

* Corresponding author at: School of Civil Engineering, Harbin Institute of Technology, Harbin 150001, China.
** Corresponding author.
E-mail addresses: lus@hit.edu.cn (S. Lu), BinPeng@usst.edu.cn (B. Peng).

http://dx.doi.org/10.1016/j.scitotenv.2022.160706
Received 18 September 2022; Received in revised form 1 December 2022; Accepted 1 December 2022
Available online 5 December 2022

Table 1
Chemical compositions of ferronickel slag and OPC (w.t%).

	SiO_2	MgO	Fe_2O_3	CaO	Al_2O_3	SO_3	Cr_2O_3	MnO	Na_2O	K_2O	TiO_2	LOI
FNS	41.77	21.17	12.52	9.49	8.03	1.78	1.70	1.11	0.48	0.34	0.27	1.34
OPC	20.94	1.70	3.44	64.02	4.85	1.88	0.50					1.88

products such as fly ash, ground granulated blast-furnace slag (GGBFS), and silica fume normally contains pozzolanic components and can be applied as the supplementary cementitious materials (SCMs) (Chi et al., 2021; Li et al., 2021; Liu et al., 2022). As a by-product of iron from the blast furnace, GGBFS possess both cementitious and pozzolanic activities. The early strength of mortar blended with GGBFS is normally lower at 3 or 7 days, however it continues to increase at 28 days and even exceeds the plain mortar (Revilla-Cuesta et al., 2022; Revilla-Cuesta et al., 2021; Santamaría et al., 2022; Sosa et al., 2022; Zhu et al., 2020). Similar to GGBFS, ferronickel slag (FNS) is an industrial solid waste produced by smelting ferronickel-iron alloy at 1000 °C–1600 °C. Every 1 t ferronickel-iron alloy produces about 6-16 t ferronickel slag (Luo et al., 2021; Xi et al., 2018). The main disposal treatment of ferronickel slag is stockpiling and landfill, resulting in land and soil degradation (Saha et al., 2018).

Since the main chemical components of ferronickel slag are SiO_2, Fe_2O_3, MgO, and chromium, ferronickel, and manganese compounds, ferronickel slag can potentially utilized as raw materials for cement clinker, SCMs, and fine aggregates (Nath et al., 2022). And there is no potential threat to environmental issues with the application of ferronickel slag in concrete, due to the leaching heavy metal ions was found to be immobilized by hydration products such as AFt, AFm or C-S-H gels in cement matrix(Cao et al., 2020). Wang Q. found that ferronickel slag has pozzolanic activity due to the large proportion of amorphous phases, which can effectively reduce the continuous pores, improve the interfacial transition zone, and be resistant to chloride penetration (Huang et al., 2017). Ashish K.S. et al. found that blending 30 % ferronickel slag as fine aggregate can improve the mechanical strength, elastic modulus, and durability of concrete, which is mainly due to the higher density attributed by better particle packing and lower voids content (Saha and Sarker, 2016; Saha and Sarker, 2017). Liu X.M. found that the hydration products of 27 % FNS blended concrete were more than that of ordinary concrete and improved the durability of concrete(Liu et al., 2020).

Compared with GGBFS, the application of ferronickel slag is limited by its chemical composition of less CaO and Al_2O_3 content, therefore, the pozzolanic activity and early hydration rate is relatively lower (Sun et al., 2019; Zhu et al., 2021a, 2021b). Lemonis et al. found that 90 d compressive strength of ferronickel slag blended cement paste would reach 90 % of pure cement paste (Saedi et al., 2020a). The activation of pozzolanic material in ferronickel slag becomes essential for the application in concrete. Therefore, it is crucial to improve the pozzolanic properties of ferronickel slag. The activation methods includes mechanical grinding, thermal activation, chemical activation, or a combination of these methods (Lemonis et al., 2015).

Hansol Kim et al. studied the effect of the grinding process on the activation of ferronickel slag and found that the reaction activity of ferronickel slag increases with a higher specific surface area (Kim et al., 2019). When the specific surface area of ferronickel slag increases from 306 m^2/kg to 558 m^2/kg, the 28d compressive strength of ferronickel slag cement mortar increases from 30.6 MPa to 36.6 MPa, and the active strength index increases from 63.4 % to 75.8 % (Wu et al., 2019). Early age steam curing can also effectively promote the formation of $(Mg, Fe)_2SiO_4$ and $MgSiO_3$ in the ferronickel slag blended cement mortar (Li et al., 2019). The chemical activation is aimed to reconstruct the atomic structure of Ca, Al, O, and Si atoms into the new amorphous network by alkaline/acid activation (Allahverdi et al., 2018; Kiventerä et al., 2018).

There are relatively few studies devoted to the early activity promotion of ferronickel slag and the hydration mechanism of ferronickel slag on concrete properties needs to be further studied. In this paper, ferronickel slag is pretreated by mechanical grinding, then the early age mechanical strength and the basic performance of ferronickel slag blended mortar is investigated. Ferronickel slag blended mortar is further thermal activation by early-age steam curing to evaluate the feasibility of the activation of the pozzolanic property.

2. Materials and methods

2.1. Characterization of ferronickel slag

The ferronickel slag tailings were from the Ferronickel-iron production plant in Jilin province. The ferronickel slag tailings are cyan irregular rocks and the mean particle size is 3–5 cm. Ferronickel slag powders with a bulk density of 2.95 g/cm^3 were dried to a constant mass at 105 °C and the moisture content in FNS is 0.4 %.

The chemical compositions of FNS were determined by X-ray fluorescence spectrometer (XRF, PANalytical Axios) and listed in Table 1. The mineral compositions of FNS were characterized using X-ray diffractometer (XRD, Rigaku D/Max-2600/PC) with a 2θ scan range of 10–75° and a scanning step of 0.02°, see Fig. 1.

Fourier transform infrared spectra of FNS was collected in KBr tablets with an FTIR-650 spectrometer in the wavenumber range of 400–4000 cm^{-1}. The morphology and crystalline observations of FNS were performed by TESCAN-VEGA3 scanning electron microscopy (CuKα radiation, 45 mA, 30 kV) with an energy dispersive spectrometer (EDS).

The ferronickel slag tailings were physically activated by grinding in a ball mill for 2 h, 5 h, and 8 h, and the specific surface areas are 493.3 m^2/kg, 530.7 m^2/kg, and 721.2 m^2/kg, correspondingly (abbreviated as AN, BN, and CN). And the particle size distributions of ferronickel slag powders with different grinding times are measured by the laser particle size analyzer (Microtrac S3500), see Fig. 2.

2.2. FNS-cement mortar preparation

Ordinary Portland cement is applied and the chemical compositions of OPC cement are present in Table 1. CEN standard sand and demineralized water is used. QSN-1000 polycarboxylate superplasticizer with an effective

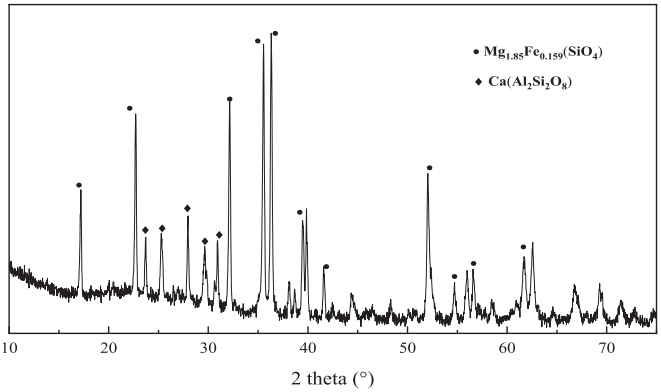

Fig. 1. XRD pattern of ferronickel slag.

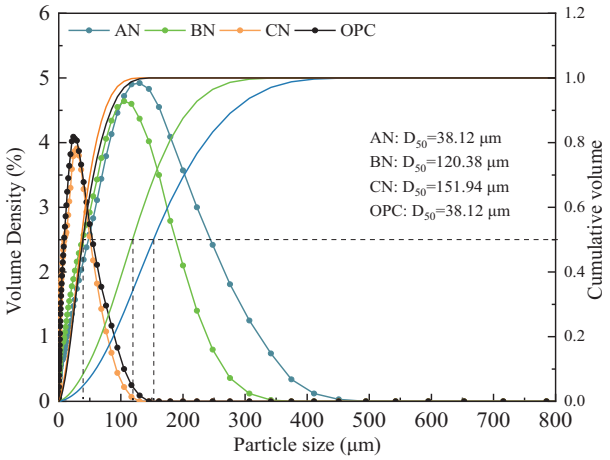

Fig. 2. Particle size distribution of ferronickel slag after mechanical grinding.

solid content of 40 % was used. In the cement mortar preparation, three specific surface areas of ferronickel slag (AN, BN, CN) correspond to different grinding times.

FNS-mortars with dimensions of 4 × 4 × 16 cm^3 were cast, demolded, and cured in the climate chamber (T = 21 ± 1 °C and RH = 65 ± 5 %) according to ASTM C109/109 M-21 (ASTM International WCP, 2019). Mix proportions of FNS-mortar are present in Table 2. A fixed water/binder-ratio = 0.45 and binder/sand-ratio = 1:3 is set for all mixes. The superplasticizer was blended 1 % relative to the total binder mass. The substitution level of ferronickel slag powder relative to the total binder mass is ranged from 0 to 40 %.

2.3. Mechanical strength, flowability, and voids of FNS-mortar

According to ASTM C109/C109M-21, the mechanical strength test of FNS-mortars was measured at 7 d and 28 d (ASTM International WCP, 2021). The flexural strength and compressive strength loading rate were set as 50 N/s and 2400 N/s, respectively. The flowability of FNS-mortars was tested according to ASTM C1437-20 (ASTM International WCP, 2020a).

Voids content of FNS-mortars were measured according to ASTM C642-13 (ASTM International WCP, 2020b). The specimens were dried in an oven set at 110 °C for 48 h, then cooled to room temperature, and weighed the mass W_0. The specimens were kept in a vacuum and then soaked in water for 18 ± 2 h. Then take out the specimens and wipe the surface of the specimens, weigh the mass of the water-saturated specimen W_1, and the mass of immersed specimen W_2. The volume of permeable voids P of FNS-mortar can be calculated according to Eq. (1).

$$P = \frac{W_1 - W_0}{W_1 - W_2} \quad (1)$$

where W_0 is the mass of the oven-dried specimen, g; W_1 is the mass of the water-saturated specimen, g; W_2 is the mass of the immersed specimens, g.

2.4. Steam curing activation

According to Standard T/ASC 01-2016, the ratio of compressive strength between cement mortar blended with 30 % SCMs and OPC cement mortar is regarded as the strength activity index (2016). Therefore, cement paste blended with 30 % BN was selected as the control group to reflect the effect of steam curing activation. The water/cement ratio was 0.45. The fresh cement paste was mixed and filled into the mould with the dimension of 40 mm × 40 mm × 40 mm. After normal temperature curing for 3 h, the samples were transferred into the steam curing chamber at normal atmospheric pressure. The steam curing temperature is set as 60 °C, 70 °C and 80 °C and the steam curing is lasted for 24 h.

2.5. Microstructure of activated FNS-mortar

The crystal structure of the FNS and the hydration products of the activated FNS-mortar are analyzed by an X-ray diffractometer (X'Pert PRO MPD) with CuKα radiation in the 2θ range 10–90° with a scanning rate of 0.02°/s and the Fourier transform infrared spectroscopy (Thermo Nicolet IS5) using KBr pellets ranging from 500 to 2000 cm^{-1}.

Surface morphology of ferronickel slag powder and the hydration products of the activated FNS-mortar are measured by Scanning Electron Microscope (HITACHI SU8010). The test voltage is 10.0 kV. The samples were freeze-dried and sprayed with gold on the surface to improve the electrical conductivity.

Thermogravimetric analysis of activated FNS-mortar is measured by DSC/TGA Discovery SDT 650 (TA instrument) heating from 0 to 1000 °C at a heat rate of 20 °C/min. 20 mg fine powder was filled in 50 μL aluminum oxide vessels. N_2 with a flow of 30 mL/min is applied as protective gas.

2.6. Life cycle assessment

The environmental impacts of the mortar's constituents mainly focus on the mix ratio and the energy consumption and emissions generated by raw materials. Therefore, the energy consumption and emissions generated by the transportation and mixing process are not considered in the life cycle assessment. The environmental impacts of the FNS-mortar are collected and listed in Table 3 according to the (Cappucci et al., 2022a; Mocharla et al., 2022; Müller et al., 2014; Norgate and Jahanshahi, 2011). The environmental impacts of the FNS-mortar can be calculated according to Eq. (1).

$$E_r = \Sigma E_{ri} * m_i \quad (1)$$

where E_{ri} represents the environmental impact of a certain material i; m_i represents the mass of certain material; E_r represents the total environmental impact.

Table 2
Mix proportions of FNS-mortars [g].

Sample ID	Cement	FNS	Sand	Water	Superplasticizer
Control	450	0	1350	202.5	4.5
FNS10	405	45			
FNS20	360	90			
FNS30	315	135			
FNS40	270	180			

Note: FNS includes AN, BN, and CN.

Table 3
Environmental impacts of the mortar's constituents (1m^3 mortar).

	Energy (kgce/t)	CO_2 (kg/t)	SO_2 kg/t	NO_x (kg/t)
Ferronickel slag	30.768	78.033	0.452	0.023
CEM I 32.5	175.710	842.000	0.500	1.533
PCE superplasticizer	0.546	0.69	0.0066	0.0035
Sand	2.389	3.7	0.0086	0.00586
Water	0.000082	0.213	0.002	0.001

3. Results and discussion

3.1. Characterization of FNS

According to XRF results, the main chemical compositions of the ferronickel slag are SiO_2, MgO, Fe_2O_3, and CaO, respectively. These phases in ferronickel slag can provide the pozzolanic activity during the hydration reaction, which is beneficial to the mechanical strength of cement-based materials. According to XRD pattern in Fig. 1, the main mineral composition of ferronickel slag is $CaAl_2Si_2O_8$, Mg_2SiO_4 and $Mg_{1.851}Fe_{0.159}(SiO_4)$. Although the magnesium content in the ferronickel slag exceeds 20 %, no diffraction peak of MgO was observed in the XRD pattern, indicating that Mg mainly exists in the form of Mg_2SiO_4 in the ferronickel slag. Mg_2SiO_4 has no significant effect on the stability of cement-based materials, which has been proved by (Xu et al., 2019). In addition, the wide diffraction peak in the XRD pattern indicates an amorphous gel phase existed in the ferronickel slag, which attributes to the hydration reaction.

According to the FT-IR pattern in Fig. 3, the peak at 3500 cm^{-1} results from the stretching vibration of hydroxyl in the water molecule. The peak in-between 800 cm^{-1} and 1100 cm^{-1} is ascribed to the Si—O stretching vibration of SiO_4^{2-} (Ma et al., 2022). The peak in-between 550 cm^{-1} and 400 cm^{-1} corresponds to the vibration and deformation of Mg—O in Mg_2SiO_4 (Li et al., 2020). Fig. 4 shows the SEM image of ferronickel slag with a smooth surface and irregular polygonal particles with a diameter of 2–10 μm. SEM-EDS analysis further confirms Mg is stable in the forms of $Mg_{1.851}Fe_{0.159}(SiO_4)$, which is consistent with XRD analysis.

The particle size distribution of the ferronickel slag grinding with different grinding times is present in Fig. 2. The particle size of ferronickel slag is decreased with the extension of grinding time. With the inducing of mechanical energy, the adhesion energy is decreased (Wei et al., 2017). And the lattice transformation, new surfaces or defects were formed in the crystalline lattice of ferronickel slag, which is contributed to the transformation to an unstable state. Therefore, the hydration reactivity can be accelerated by mechanical activation with a relatively small particle size(Yao et al., 2019a).

3.2. Flowability of FNS-mortar

Fig. 5 shows the flowability of FNS-mortars with different fineness (AN, BN, CN) and mixture content (0 %–40 %), There is no segregation occurs with all the proportions, see Fig. 6. With the increase of ferronickel slag content and fineness, the flowability of cement mortar continues to improve, and the maximum increase of flowability reaches 81.0 % for CN40

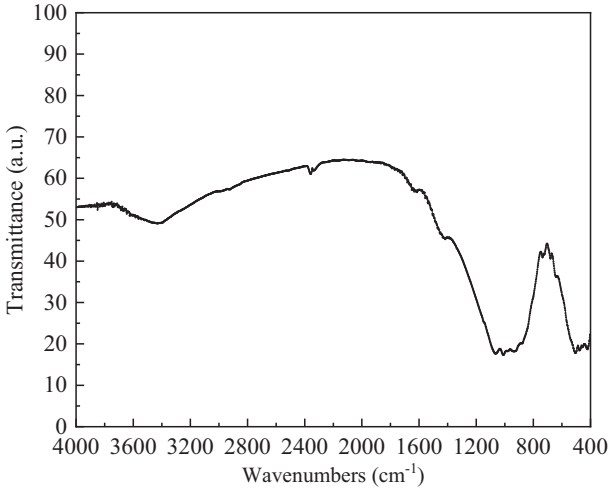

Fig. 3. FT-IR spectra of ferronickel slag.

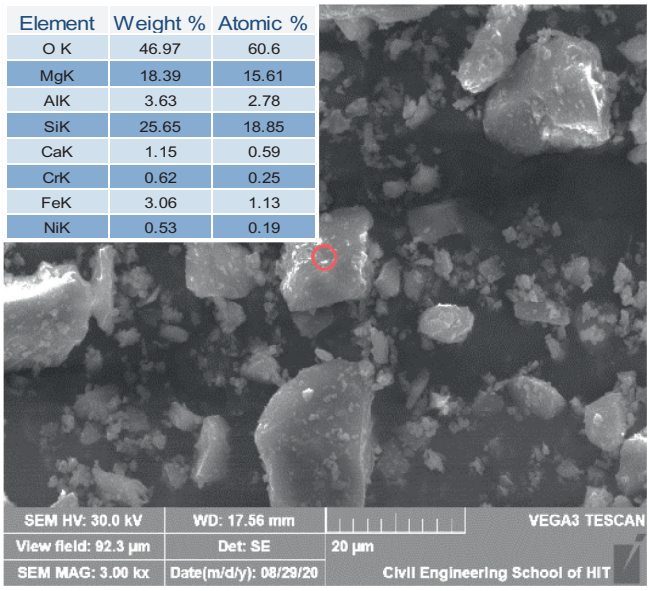

Fig. 4. SEM-EDS analysis of ferronickel slag.

mortar. This is mainly due to with the increase of ferronickel slag content in mortar, the proportion of charged particles per unit volume in cement mortar decreases correspondingly, and the inter-molecular forces and friction between cement particles decrease, leading to the improvement of flowability (Wu et al., 2019). With the higher specific surface area of ferronickel slag, the flowability of cement mortar is also increased. As a fine particle, ferronickel slag can fill the gaps between cement particles and sand, and the distance between cement particles is enlarged, thus increasing the flowability of mortar.

3.3. Permeable voids of FNS-mortar

The voids of FNS-mortars with different fineness and content (10 %–40 %) at 28d were present in Fig. 7 and Table 4. Since cement mortar is a heterogeneous cementitious material with a complex pore structure, the interfaces between the hardened cement matrix and sand becomes a channel for external ions to exchange, transmit and diffuse inside cement-based materials, which easily induce durability damage and strength loss (Yang et al., 2020). The results indicate that ferronickel slag content is proportional to the permeable voids of the FNS-mortar.

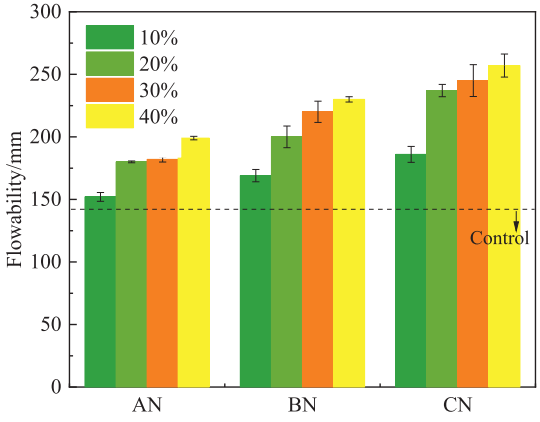

Fig. 5. Flowability of FNS-mortar blended with different FNS.

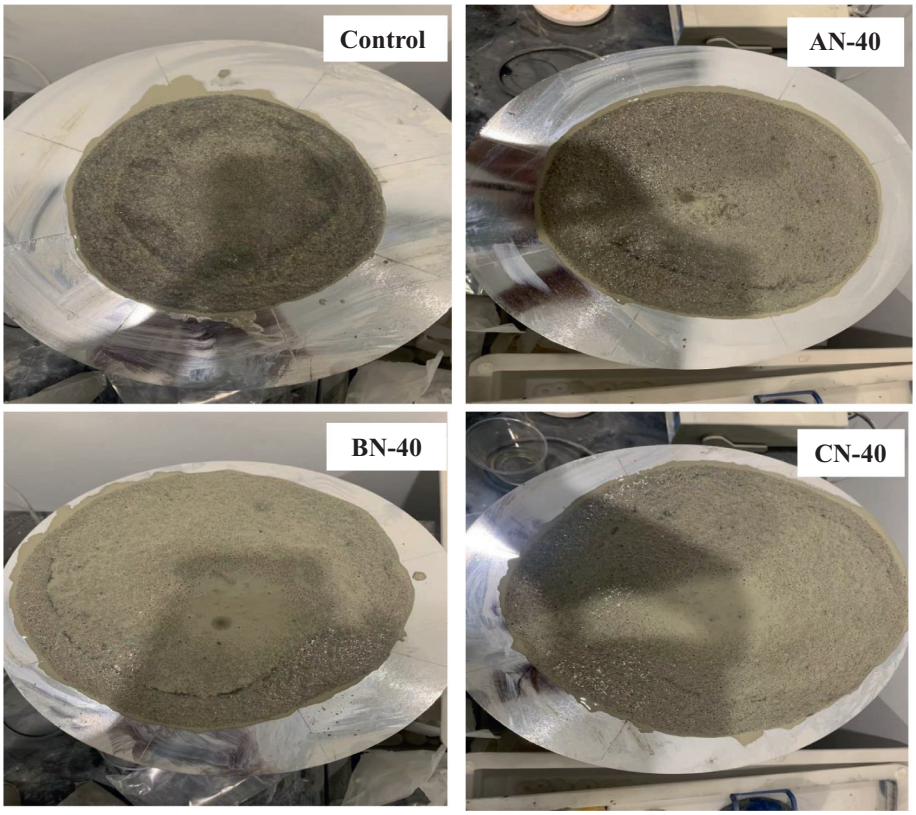

Fig. 6. Flowability test of FNS-mortar.

Considering the same mixing proportion of FNS, the permeable void of AN-morta is larger than CN-mortar, then follows the BN-mortar. With more grounding time, the specific area of CN is larger than BN. The excessive grinding may lead to agglomeration of particles hindering the mechanical strength of mortar. The particle size distribution of CN is almost same with cement particles, the particle size distribution of BN is in the middle of cement and sand. Therefore, it can be deduced that the particle size of BN is more benefit to the close packing of cement mortar. Mechanical grinding process contributes to the activation of FNS, however, there is a limitation for mechanical grinding time in case of leading to the agglomeration of superfine particles.

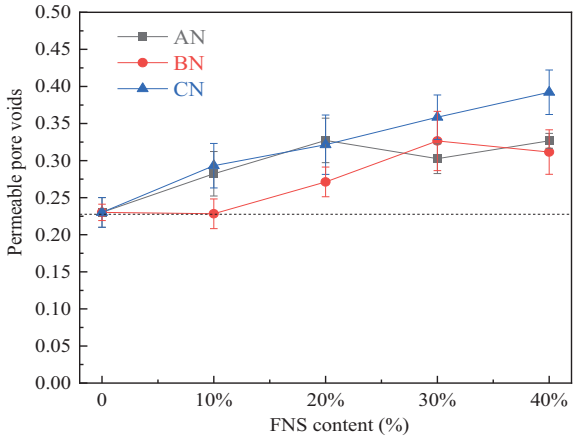

Fig. 7. Permeable pore voids of FNS-mortar at 28d.

3.4. Mechanical strength of FNS-mortar

The mechanical strength measurement of FNS-mortars with different fineness (AN, BN, CN) and content (10 %–40 %) at 7d and 28d were present in Fig. 8. With the increasing proportion of ferronickel slag, the flexural strength of FNS-mortar decreased at different levels, see Fig. 8 a) and b). At the age of 7 d, the flexural strength of FNS-mortar decreases significantly, particularly the decline of AN- and CN-mortar exceeds 40 %. At the age of 28 d, the flexural strength of AN10 or CN10 mortar decreases 12.5 % or 0.7 %, and the flexural strength of BN10 or BN20 mortar increases 17 % or 2.2 %.

The compressive strength of FNS-mortar at 7d or 28d is shown in Fig. 8 c) and d). With the increasing proportion of ferronickel slag, the compressive strength of FNS-mortar decreased in proportion at the age of 7 d.

Table 4
Voids content of FNS-mortar with different fineness and content.

Sample ID	Dry mass (g)	Saturated mass (g)	Immersed mass (g)	Air voids content
Control	201.67	226.72	117.88	0.230
AN10	214.8	249.98	125.34	0.282
AN20	211.77	254.47	123.98	0.327
AN30	201.27	237.42	117.95	0.303
AN40	197.55	236.21	117.88	0.327
BN10	234.85	264.45	134.80	0.228
BN20	203.79	235.42	118.81	0.271
BN30	184.74	221.81	108.27	0.326
BN40	230.58	273.57	135.56	0.312
CN10	198.09	233.61	112.42	0.293
CN20	206.11	247.68	118.37	0.321
CN30	194.18	238.38	115.11	0.359
CN40	190.91	239.72	115.25	0.392

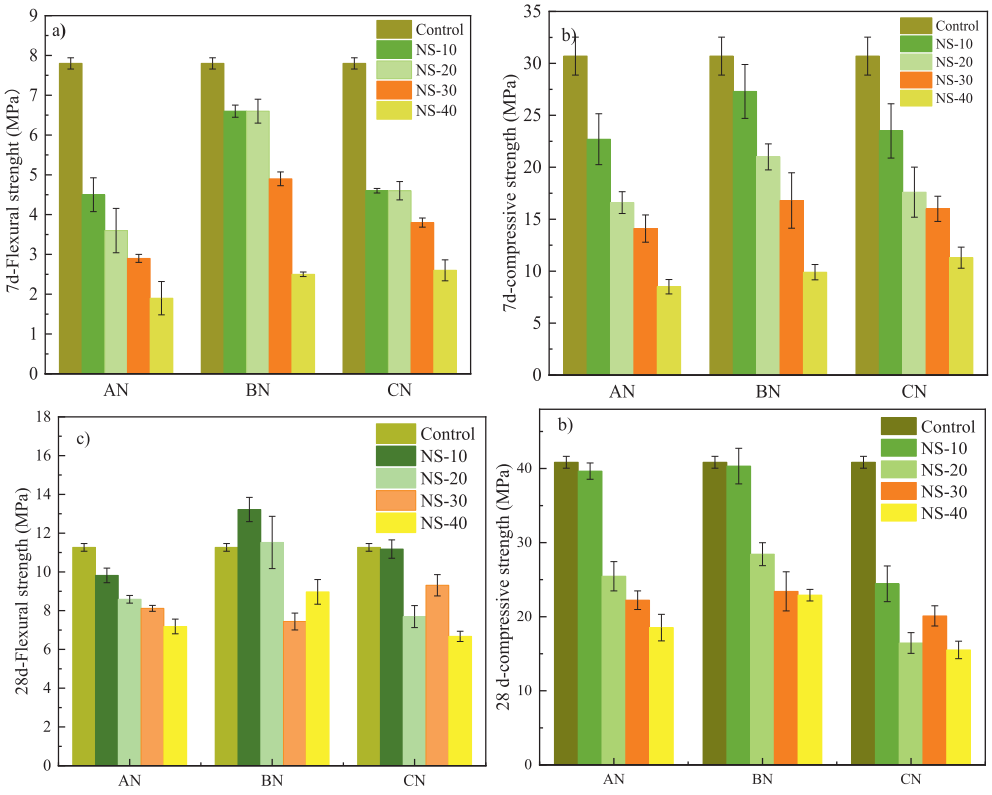

Fig. 8. Mechanical strength of FNS cement mortar at 7 d and 28 d.

With a relatively lower FNS content, the compressive strength of AN10 or BN10 mortar remains the same at 28d. With 20 % FNS-content, the decline of all proportions of FNS-mortar is more than 30 %, even up to 61.7 %. Considering the effect of fineness of FNS, the compressive strength of BN mortar is the largest, followed by CN- and AN-mortar. This is mainly due to the relatively larger particle size, the activated components in the AN-ferronickel slag are not easily released and participated in the hydration reaction process. Correspondingly, the crystallinity of main mineral phases in BN- and CN-ferronickel slag is decreased by mechanical grinding, the activity of mechanically activated BN- and CN-ferronickel slag is gradually increased with grinding time (Yao et al., 2019b). In addition, considering the principle of closest packing of spheres, BN-ferronickel slag can fill the tiny gap between cement particles and sand, resulting in the highest mechanical strength. Considering the results of flowability and mechanical strength of FNS-mortar, 10 % ferronickel slag relative to the total binder mass is the optimal mix proportion of the system. It can be concluded that with mechanically activated FNS content exceeding 10 %, further activation treatments should be applied to increase the pozzolanic activity.

3.5. Pozzolanic activity property of ferronickel slag in FNS-mortar

According to Chinese Standard (2016), if the ratio of compressive strength at 7d and 28d is higher than 0.65 and 0.75, ferronickel slag is considered to have volcanic activity and can participate in cement hydration. The strength activity index can be calculated according to Eq. (2) (Saha et al., 2019).

$$K = \frac{R_1}{R_2} \tag{2}$$

where K is the ratio of compressive strength, %; R_1 is the compressive strength of FNS-mortar, MPa; R_2 is the compressive strength of OPC cement mortar, MPa.

Table 5 shows the pozzolanic activity property of ferronickel slag in FNS-mortar at the age of 7d and 28d. The results show that the ratio of compressive strength of FNS-mortar AN10, BN10, BN20, and CN10 at 7d exceeds 65 %, and the ratio of compressive strength of FNS-mortar AN10 and BN10 at 28d exceeds 85 %. It can be concluded that the 28d-compressive strength of FNS-mortar with low ferronickel slag content remains the same, however, the early age compressive strength is reduced. According to the strength activity index for ferronickel slag in the standard T/ASC 01–2016, only AN10 and BN10 can meet the requirement simultaneously, which indicates that most of the ferronickel slag did not participate in the cement hydration reaction but only did for close packing of the particle.

Table 5
Pozzolanic activity property of ferronickel slag in FNS-mortar.

Group	Compressive strength (MPa)		Pozzolanic activity index	
	7d	28 d	7d	28 d
Control	30.72	40.85	–	–
AN10	22.73	39.66	0.74	0.96
AN20	16.67	25.46	0.54	0.62
AN30	14.14	22.23	0.46	0.54
AN40	8.56	18.53	0.28	0.45
BN10	27.32	40.34	0.89	0.99
BN20	21.54	28.44	0.68	0.70
BN30	16.82	23.42	0.55	0.57
BN40	9.94	22.91	0.32	0.56
CN10	23.51	24.44	0.77	0.60
CN20	17.6	16.45	0.57	0.40
CN30	16	20.11	0.52	0.49
CN40	11.3	15.52	0.37	0.38

3.6. Performance of steam-cured BN-cement paste

Compared with plain cement mortar, with a relatively higher percentage of ferronickel slag content, the mechanical strength of cement mortar is declined. Due to the performance of cement-based materials with high volume SCMs can be accelerated by a steam curing procedure (Yang et al., 2014), therefore, early-age steam curing pretreatment is applied to activate the ferronickel slag. Fig. 9 shows the compressive strength and porosity of BN-cement paste cured at 20 °C, 60 °C, 70 °C and 80 °C. The connected porosity of the cement paste blended with BN is increased due to the low hydration activity of BN at an early age, which is consistent with literature results (Karen et al., 2018). With the increase of steam curing temperature, the connected porosity of cement-based materials decreases significantly, which indicates the accelerated secondary hydration and the cumulative of hydration products filling the pores(Nguyen et al., 2020). Compared with 30 % BN-paste with standard curing, the compressive strength of hardened BN-cement paste with steam curing ranging from 60 °C to 80 °C increased from 8.2 % to 33.8 %, and the connected porosity decreased from 18.9 % to 17.3 %. The increased rate of porosity and compressive strength of FNS-paste slows down with the temperature rises from 60 °C to 80 °C.

Considering the same steam curing temperature, the compressive strength of BN30 is lower than that of control, such as Control-20 and BN-30-20, Control-60 and BN-30-60, and Control-80 and BN-30-80. However, the compressive strength of 30 % FNS-paste with steam curing at 80 °C is basically the same as that of standard-cured control sample. It can be concluded that although the addition of FNS would decrease the compressive strength of FNS-paste, the steam curing would promote the secondary hydration of FNS and compensate for loss of strength. It is further proved that high temperature steam curing is the key step to promote the application of ferronikel slag in the cement-based materials.

3.7. Microstructure of FNS-mortar

3.7.1. XRD analysis

Fig. 10 shows the XRD patterns of early-age steam cured FNS-30 cement paste at 28d. Compared with normal curing conditions, the characteristic diffraction peaks of pure cement paste with steam curing at 60 °C, 70 °C and 80 °C are identical, indicating less effect on the hydration products of pure cement paste with steam curing. The hydration products of FNS-cement paste mainly include $Ca(OH)_2$, AFm, unhydrated cement phase (Zhu et al., 2021a, 2021b; Zulhan and Agustina, 2021). With the curing temperature increasing, the diffraction peak of calcium hydroxide decreases obviously in the FNS30 samples steaming curing at 80 °C. The diffraction peak of magnesium silicate can be detected in the XRD pattern of FNS-30 cement paste, which indicates the ferronickel slag cannot completely participate in the hydration reaction when the temperature was raised during steam curing. Despite the high MgO content in ferronickel slag, no diffraction peak of $Mg(OH)_2$ was found in hydration products which is due to the magnesium existence in the form of (Mg, Fe)$_2SiO_4$ and $MgSiO_3$ (Choi and Choi, 2015). It is noted that early age steam curing promotes the reaction between SiO_2, Fe_2O_3, Al_2O_3 and $Ca(OH)_2$, then further accelerate the cement hydration process.

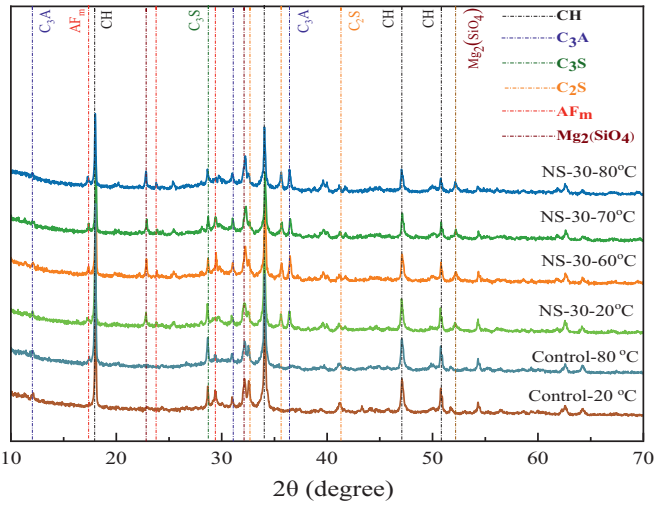

Fig. 10. XRD patterns of FNS-cement paste with steam curing at 60 °C, 70 °C and 80 °C.

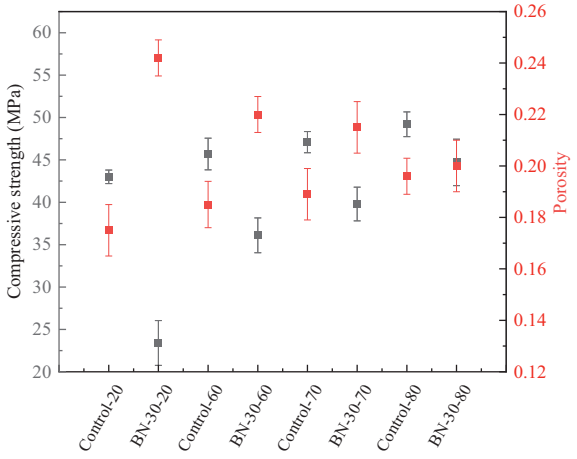

Fig. 9. Compressive strength and porosity of BN-cement paste with steam curing at 60 °C, 70 °C and 80 °C.

3.7.2. DTG-TG analysis

Fig. 11 shows the DTG-TG curve and heat flow curve of early-age steam cured FNS-30 cement paste at 28d. As observed in Fig. 11, the dehydroxylation peak between 370 °C and 460 °C represents portlandite (CH), and the decarbonization peaks between 600 °C and 1000 °C represent the decomposition of calcite ($CaCO_3$) (Wang et al., 2022). And the weight loss between 100 °C and 370 °C is due to the dehydroxylation of AFt and AFm. The CH content is decreased with the addition of ferronickel slag in cement paste. And with a relatively higher steam curing temperature of 80 °C, the CH content decreases by 8.39 %. It indicates that the steam curing can effectively promote the hydration activity of ferronickel slag with CH during the secondary hydration reaction.

3.7.3. SEM image analysis

Fig. 12 and Table 6 show the SEM images and EDAX results of early-age steam cured FNS-30 cement paste at 28d. More lamellar hydrotalcite can be recognized from the SEM image of FNS-30 cement paste, which is due to the steam curing promoting the formation of hydrotalcite and the transition of AFt into AFm(Li et al., 2019). Mg can be detected in C-S-H gels of FNS-30-20 °C cement mortar. And the Mg content of C-S-H gels of FNS-30 cement mortar ranges from 1 % to 9 % with the steam curing temperature ranging from 20 °C-80 °C. It indicates that Mg from ferronickel slag would enter the C-S-H microstructure and forms M-S-H gel. And it is consistent with the observation of the rehydration effect leading to the consumption of CH derived from XRD and DTG results.

3.8. Life cycle assessment of FNS-mortar

As a potential cementitious materials, ferronickel slag would contribute to promote the solid waste utilization with the application in the concrete

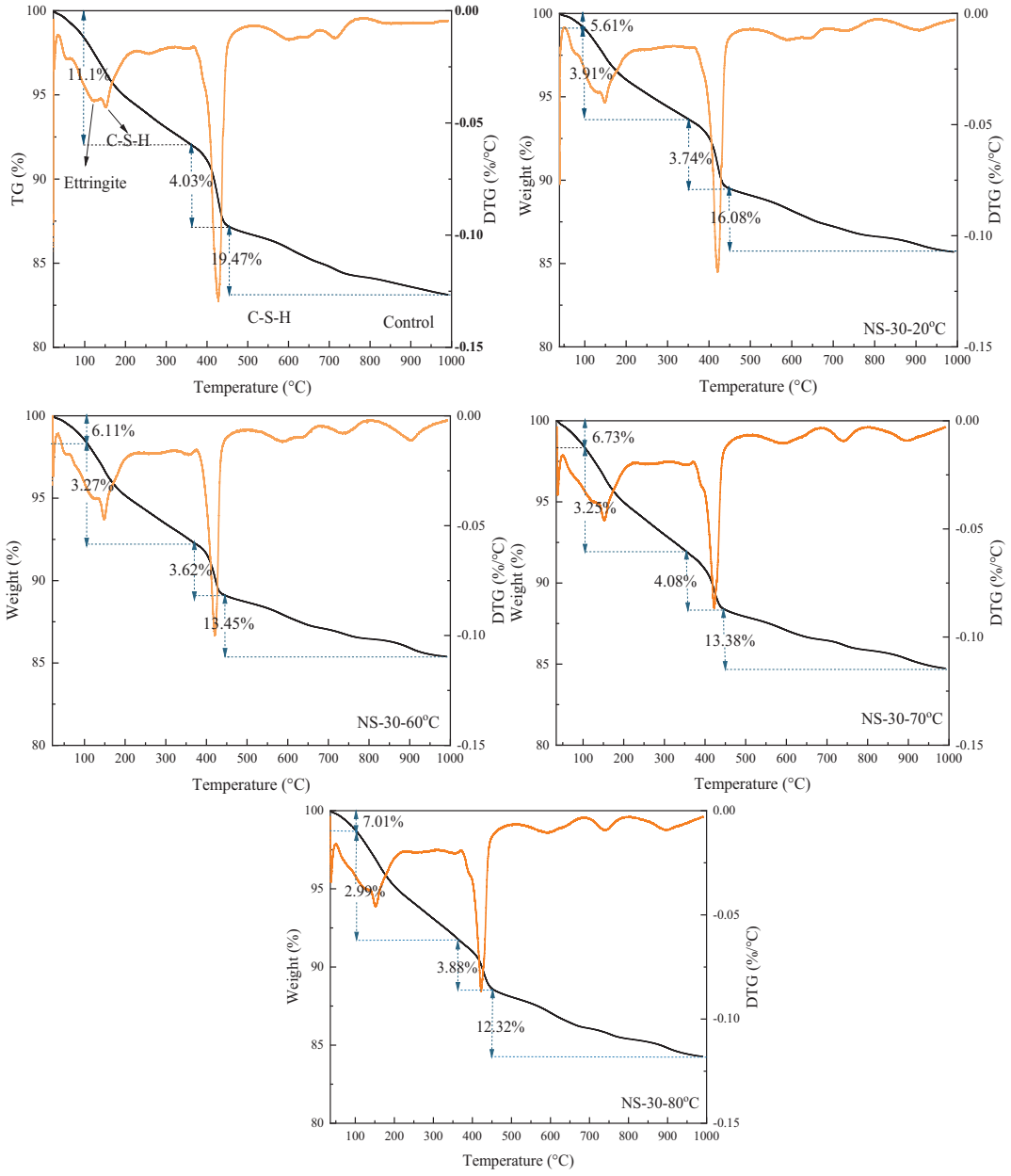

Fig. 11. DTG-TG curve of FNS-cement paste with different curing temperatures.

or cement-based materials. And due to the large content of olivine and high hardness of ferronickel slag, the application of ferronickel slag as fine aggregate in cement mortar improves the wear resistance of cement-based materials, which can be further applied in the embankment or pavement materials. According to the energy consumption, CO_2 emissions, SO_x emissions, and NO_x generated by the raw materials of FNS-mortar, the life cycle assessment of ferronickel slag cement-based materials was explored and present in Fig. 13. The blended ferronickel slag in cement-based materials can effectively reduce energy consumption, CO_2 emissions, SO_x emissions, and NO_x emissions(Matthias et al., 2006). With 40 % FNS blended, energy consumption is reduced by 31.70 %, CO_2 emissions by 35.82 %, NO_x emissions by 38.94 %, and SO_x emissions by 3.61 %. With the increase of blending content, the energy consumption of ferronickel slag cement mortar and the overflow ratio of gas emissions are gradually reduced compared with pure cement mortar. Based on the environmental assessment, FNS10 mortar possesses the optimal performance and least environmental impact. Compared with other SCMs, the limitation is the proportion of FNS in cement mortar is relatively low, therefore, it is necessary to apply the combined activation pretreatment on the high proportion FNS. In practical application, with further physical grinding and steam curing, FNS is substituted to fine aggregate in concrete. The amount of FNS replacing sand is about 0.3 ton/m^2 on average. The price of nickel slag is 25 yuan cheaper than that of sand per ton, saving 7.5 yuan for each cubic concrete (Cappucci et al., 2022b). Previous study confirms that concrete with steam curing in range of 45–80 °C and lasting for 24 h can promote the concrete properties, especially for high proportion of SCMs (Zeyad et al., 2022). Comparing with the CO_2 emission or energy consumption of steam curing, the high-temperature calcining and grinding process of cement clinker is hundreds of time larger(Saedi et al., 2020b). Therefore, the utilization of FNS in the future research area is mainly focused on the low energy activation with physical or chemical treatment such as microwave activation or infrared activation, etc.

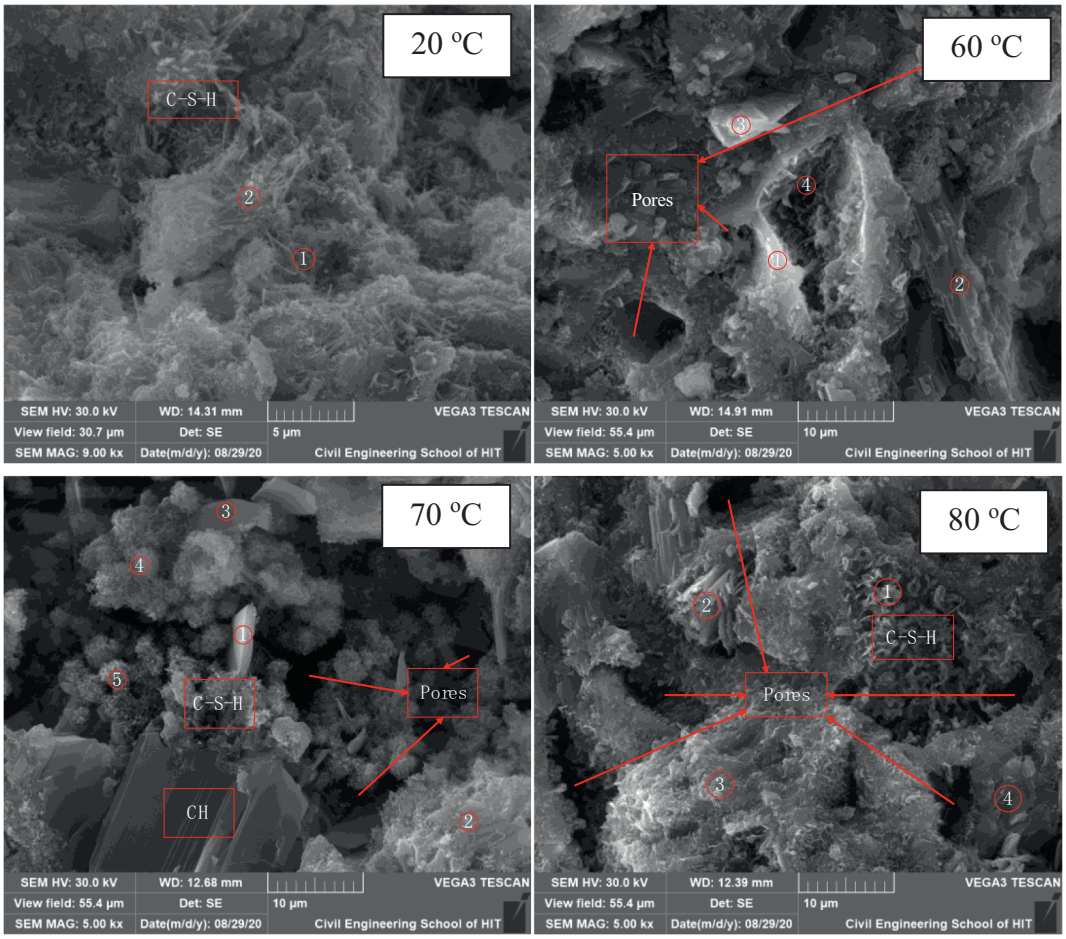

Fig. 12. SEM images of FNS-cement paste with different curing temperature.

4. Conclusions

This study investigates the early activity promotion of ferronickel slag and the hydration mechanism of ferronickel slag on mortar properties. And the following conclusions can be drawn as follows.

(1) Ferronickel slag can effectively improve the flowability of mortar and air voids content. Pozzolanic activity property results indicate that ferronickel slag with more than 10 % barely participates in the cement hydration reaction in the early stage, and the mechanical strength of FNS-mortar decreases with the higher proportion of ferronickel slag.

Table 6
EDAX results of FNS-cement paste with different curing temperature.

Atomic	(%)	O	Mg	Al	Si	S	Ca	Fe
FNS-30-20	Plot1	64.51	6.02	2.41	10.99	2.51	12.31	1.25
	Plot2	64.84	4.29	3.43	8.62	2.34	14.62	1.87
FNS-30-60	Plot1	64.6	3.56	8.98	3.63	1.98	16.06	1.18
	Plot2	56.74	3.82	0.9	4.58	2.23	30.96	0.76
	Plot3	62.93	19.56	0.9	12.47	1.38	1.98	0.78
	Plot4	45.12	2.43	1.73	4.89	3.65	38.46	3.72
FNS-30-70	Plot1	68.37	3.49	4.38	5.5	5.35	12.11	0.79
	Plot2	62.98	11.64	1.94	13.03	1.64	8.11	0.95
	Plot3	73.02	2.27	3.58	4.01	4.14	12.06	0.9
	Plot4	71.74	4.35	1.23	7.19	3.4	10.8	1.28
	Plot5	72.05	4.58	1.28	7.41	2.52	11.45	0.71
FNS-30-80	Plot1	60.43	5.21	2.55	10.75	3.05	16.61	1.4
	Plot2	41.99	1.56	1.99	14.12	2.5	36.53	1.3
	Plot3	55.91	5.3	2.84	11.59	3.97	18.37	2.01
	Plot4	50.61	9.08	3.83	14.44	3.79	16.41	1.84

(2) The activation of pozzolanic material in ferronickel slag can effectively be improved by mechanical grinding and steam curing at an early age. The excessive grinding may lead to agglomeration of particles hindering the mechanical strength of mortar. Compared with standard curing, the compressive strength of hardened FNS-cement paste with steam curing at 60 °C or 80 °C increased by 8.2 % or 33.8 %, and the connected porosity decreased by 18.9 % or 17.3 %.

(3) MgO in the ferronickel slag exists as Mg_2SiO_4 in raw materials and enters the C-S-H gel with the formation of M-S-H gel during the secondary hydration stage, which can prove that the ferronickel slag can be applied as the SCMs in cement-based materials irrespective of stability issue.

(4) The blended ferronickel slag in cement-based materials can effectively reduce energy consumption, CO_2 emissions, SO_x emissions, and NO_x emissions. With 40 % FNS blended, energy consumption is reduced by 31.70 %, CO_2 emissions by 35.82 %, NO_x emissions by 38.94 %, and SO_x emissions by 3.61 %.

CRediT authorship contribution statement

Lin Chi: Conceptualization, Writing-original draft, Funding acquisition. Jiang Hui: Data analysis, Visualization; Shuang Lu: Supervision, Funding acquisition; Zheming Li: Formal analysis,Writing - Review & Editing; Chengdong Huang: Validation, Data Curation; Bin Peng: Supervision, Funding acquisition.

Data availability

Data will be made available on request.

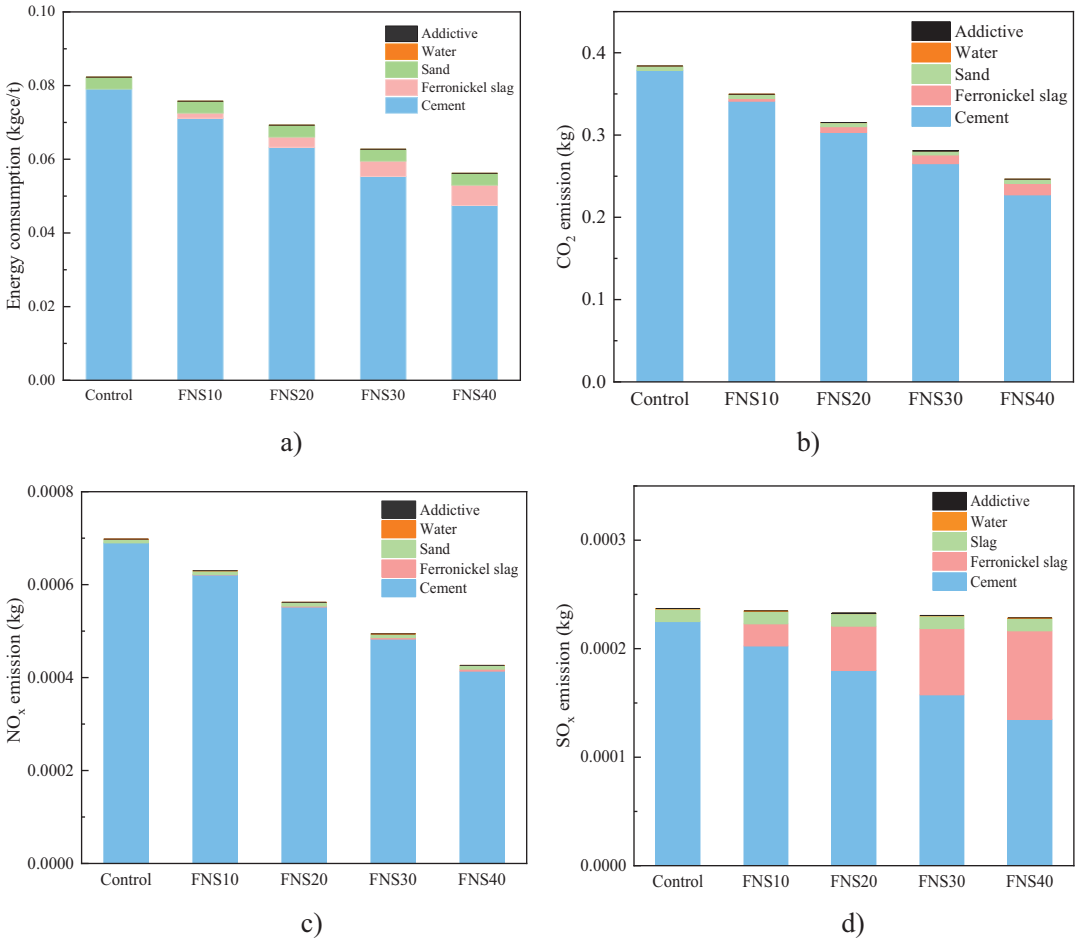

Fig. 13. The environmental impact (normalized) of FNS-mortar.

Declaration of competing interest

The authors declare no conflict of interest. This article does not contain any studies with human participants or animals performed by any of the authors. Informed consent was obtained from all individual participants included in the study.

Acknowledgments

This work was supported by the National Natural Science Foundation of China (No. 52208269, No. 51872064, No. 52178196, No.51978401), Shanghai Sailing Program (No.20YF1431800), Key Laboratory of Performance Evolution and Control for Engineering Structures (Tongji University), No. 2019KF-5 and the Open Fund of Shanghai Key Laboratory of Engineering Structure Safety, No. 2019-KF07.

References

Allahverdi, A., Maleki, A., Mahinroosta, M., 2018. Chemical activation of slag-blended Portland cement. J. Build. Eng. 18, 76–83.
ASTM International WCP, 2019. Standard Test Methods for Time of Setting of Hydraulic Cement by Vicat Needle. ASTM C191-19, p. 462.
ASTM International WCP, 2020. Standard Test Method for Flow of Hydraulic Cement Mortar. ASTM C1437-20, p. 253.
ASTM International WCP, 2020. Standard Test Method for Density, Absorption, and Voids in Hardened Concrete. ASTM C642-13, p. 28.
ASTM International WCP, 2021. Standard Test Method for Compressive Strength of Hydraulic Cement Mortars (Using 2-in. or [50 mm] Cube Specimens). ASTM C109/C109M-21, p. 57.
Cao, R., Jia, Z., Zhang, Z., Zhang, Y., Banthia, N., 2020. Leaching kinetics and reactivity evaluation of ferronickel slag in alkaline conditions. Cem. Concr. Res. 137, 106202.
Cappucci, G.M., Ruffini, V., Barbieri, V., Siligardi, C., Ferrari, A.M., 2022a. Life cycle assessment of wheat husk based agro-concrete block. J. Clean. Prod. 349, 131437.
Cappucci, G.M., Ruffini, V., Barbieri, V., Siligardi, C., Ferrari, A.M., 2022b. Life cycle assessment of wheat husk based agro-concrete block. J. Clean. Prod. 349, 131437.
Chi, L., Wang, Z., Lu, S., Wang, H., Liu, K., Liu, W., 2021. Early assessment of hydration and microstructure evolution of belite-calcium sulfoaluminate cement pastes by electrical impedance spectroscopy. Electrochim. Acta 389, 138699.
Chinese Standard, 2016. Ferronickel Slag Powder for Cement and Concrete. T/ASC-2016, p. 14.
Choi, Y.C., Choi, S., 2015. Alkali–silica reactivity of cementitious materials using ferro-nickel slag fine aggregates produced in different cooling conditions. Constr. Build. Mater. 99, 279–287.
Gartner, E., Hirao, H., 2015. A review of alternative approaches to the reduction of CO2 emissions associated with the manufacture of the binder phase in concrete. Cem. Concr. Res. 78, 126–142.
Huang, Y., Wang, Q., Shi, M., 2017. Characteristics and reactivity of ferronickel slag powder. Constr. Build. Mater. 156, 773–789.
Kaliyavaradhan, S.K., Ling, T., Mo, K.H., 2020. Valorization of waste powders from cement-concrete life cycle: a pathway to circular future. J. Clean. Prod. 268, 122358.
Karen, S., Ruben, S., Barbara, L., 2018. A Practical Guide to Microstructural Analysis of Cementitious Materials. CRC Press.
Kim, H., Lee, C.H., Ann, K.Y., 2019. Feasibility of ferronickel slag powder for cementitious binder in concrete mix. Constr. Build. Mater. 207, 693–705.
Kiventerä, J., Lancellotti, I., Catauro, M., Poggetto, F.D., Leonelli, C., Illikainen, M., 2018. Alkali activation as new option for gold mine tailings inertization. J. Clean. Prod. 187, 76–84.
Lemonis, N., Tsakiridis, P.E., Katsiotis, N.S., Antiohos, S., Papageorgiou, D., Katsiotis, M.S., et al., 2015. Hydration study of ternary blended cements containing ferronickel slag and natural pozzolan. Constr. Build. Mater. 81, 130–139.
Li, B., Huo, B., Cao, R., Wang, S., Zhang, Y., 2019. Sulfate resistance of steam cured ferronickel slag blended cement mortar. Cem. Concr. Compos. 96, 204–211.
Li, Z., Lu, T., Liang, X., Dong, H., Ye, G., 2020. Mechanisms of autogenous shrinkage of alkali-activated slag and fly ash pastes. Cem. Concr. Res. 135, 106107.
Li, Z., Alfredo Flores Beltran, I., Chen, Y., Šavija, B., Ye, G., 2021. Early-age properties of alkali-activated slag and glass wool paste. Constr. Build. Mater. 291, 123326.
Liu, J., Liang, Z., Jin, H., Kastiukas, G., Tang, L., Xing, F., et al., 2022. Alkali-activated binders based on incinerator bottom ash combined with limestone-calcined clay or fly ash. Constr. Build. Mater. 320, 126306.
Liu, X., Li, T., Tian, W., Wang, Y., Chen, Y., 2020. Study on the durability of concrete with FNS fine aggregate. J. Hazard. Mater. 381, 120936.
Luo, J., Li, G., Rao, M., Peng, Z., Liang, G., Jiang, T., et al., 2021. Control of slag formation in the electric furnace smelting of ferronickel for an energy-saving production. J. Clean. Prod. 287, 125082.

Ma, H., Zhang, S., Feng, J., 2022. Early hydration properties and microstructure evolutions of MgO-activated slag materials at different curing temperatures. Ceram. Int. 48, 17104–17115.
Matthias, F., Atsushi, I., Reginald, T., Kim, C., Hans-Jürgen, K., 2006. The new international standards for life cycle assessment: ISO 14040 and ISO 14044. Int. J. Life Cycle Assess. 11.
Mocharla, I.R., Selvam, R., Govindaraj, V., Muthu, M., 2022. Performance and life-cycle assessment of high-volume fly ash concrete mixes containing steel slag sand. Constr. Build. Mater. 341, 127814.
Müller, H.S., Breiner, R., Moffatt, J.S., Haist, M., 2014. Design and properties of sustainable concrete. Procedia Eng. 95, 290–304.
Nath, S.K., Randhawa, N.S., Kumar, S., 2022. A review on characteristics of silico-manganese slag and its utilization into construction materials. Resour. Conserv. Recycl. 176, 105946.
Nguyen, M.H., Nakarai, K., Torrent, R., 2020. Service life prediction of steam-cured concrete utilizing in-situ air permeability measurements. Cem.Concr.Compos. 114, 103747.
Norgate, T., Jahanshahi, S., 2011. Assessing the energy and greenhouse gas footprints of nickel laterite processing. Miner. Eng. 24, 698–707.
Revilla-Cuesta, V., Skaf, M., Serrano-López, R., Ortega-López, V., 2021. Models for compressive strength estimation through non-destructive testing of highly self-compacting concrete containing recycled concrete aggregate and slag-based binder. Constr. Build. Mater. 280.
Revilla-Cuesta, V., Ortega-López, V., Skaf, M., Khan, A., Manso, J.M., 2022. Deformational behavior of self-compacting concrete containing recycled aggregate, slag cement and green powders under compression and bending: description and prediction adjustment. J.Build. Eng. 54, 104611.
Saedi, A., Jamshidi-Zanjani, A., Darban, A.K., 2020a. A review on different methods of activating tailings to improve their cementitious property as cemented paste and reusability. J. Environ. Manag. 270, 110881.
Saedi, A., Jamshidi-Zanjani, A., Darban, A.K., 2020b. A review on different methods of activating tailings to improve their cementitious property as cemented paste and reusability. J. Environ. Manag. 270, 110881.
Saha, A.K., Sarker, P.K., 2016. Expansion due to alkali-silica reaction of ferronickel slag fine aggregate in OPC and blended cement mortars. Constr. Build. Mater. 123, 135–142.
Saha, A.K., Sarker, P.K., 2017. Sustainable use of ferronickel slag fine aggregate and fly ash in structural concrete: mechanical properties and leaching study. J. Clean. Prod. 162, 438–448.
Saha, A.K., Khan, M.N.N., Sarker, P.K., 2018. Value added utilization of by-product electric furnace ferronickel slag as construction materials: a review. Resour. Conserv. Recycl. 134, 10–24.
Saha, A.K., Sarker, P.K., Golovanevskiy, V., 2019. Thermal properties and residual strength after high temperature exposure of cement mortar using ferronickel slag aggregate. Constr. Build. Mater. 199, 601–612.
Santamaría, A., Romera, J.M., Marcos, I., Revilla-Cuesta, V., Ortega-López, V., 2022. Shear strength assessment of reinforced concrete components containing EAF steel slag aggregates. J.Build.Eng. 46, 103730.
Shi, C., Wu, Y., 2008. Studies on some factors affecting CO2 curing of lightweight concrete products. Resour. Conserv. Recycl. 52, 1087–1092.
Sosa, I., Thomas, C., Polanco, J.A., Setién, J., Sainz-Aja, J.A., Tamayo, P., 2022. Durability of high-performance self-compacted concrete using electric arc furnace slag aggregate and cupola slag powder. Cem. Concr. Compos. 127, 104399.
Sun, J., Feng, J., Chen, Z., 2019. Effect of ferronickel slag as fine aggregate on properties of concrete. Constr. Build. Mater. 206, 201–209.
Wang, Y., Wang, W., Ma, M., He, X., Su, Y., Strnadel, B., et al., 2022. Microstructure and mechanical properties of activated high-alumina ferronickel slag with carbide slag and alkaline salts. J. Build. Eng. 49, 104046.
Wei, B., Zhang, Y., Bao, S., 2017. Preparation of geopolymers from vanadium tailings by mechanical activation. Constr. Build. Mater. 145, 236–242.
Wu, Q., Wang, S., Yang, T., Zhu, H., Li, S., 2019. Effect of high-magnesium nickel slag on hydration characteristics of Portland cement. J. Mater. Civ. Eng. 31.
Xi, B., Li, R., Zhao, X., Dang, Q., Zhang, D., Tan, W., 2018. Constraints and opportunities for the recycling of growing ferronickel slag in China. Resour. Conserv. Recycl. 139, 15–16.
Xu, W., Chen, J.J., Wei, J., Zhang, B., Yuan, X., Xu, P., et al., 2019. Evaluation of inherent factors on flowability, cohesiveness and strength of cementitious mortar in presence of zeolite powder. Constr. Build. Mater. 214, 61–73.
Yang, T., Yao, X., Zhang, Z., 2014. Geopolymer prepared with high-magnesium nickel slag: characterization of properties and microstructure. Constr. Build. Mater. 59, 188–194.
Yang, T., Zhang, Z., Wang, Q., Wu, Q., 2020. ASR potential of nickel slag fine aggregate in blast furnace slag-fly ash geopolymer and Portland cement mortars. Constr. Build. Mater. 262, 119990.
Yao, G., Liu, Q., Wang, J., Wu, P., Lyu, X., 2019a. Effect of mechanical grinding on pozzolanic activity and hydration properties of siliceous gold ore tailings. J. Clean. Prod. 217, 12–21.
Yao, G., Liu, Q., Wang, J., Wu, P., Lyu, X., 2019b. Effect of mechanical grinding on pozzolanic activity and hydration properties of siliceous gold ore tailings. J. Clean. Prod. 217, 12–21.
Zeyad, A.M., Tayeh, B.A., Adesina, A., de Azevedo, A.R.G., Amin, M., Hadzima-Nyarko, M., et al., 2022. Review on effect of steam curing on behavior of concrete. Clean. Mater. 3, 100042.
Zhu, X., Zhang, M., Yang, K., Yu, L., Yang, C., 2020. Setting behaviours and early-age microstructures of alkali-activated ground granulated blast furnace slag (GGBS) from different regions in China. Cem. Concr. Compos. 114, 103782.
Zhu, X., Kang, X., Deng, J., Yang, K., Jiang, S., Yang, C., 2021. Chemical and physical effects of high-volume limestone powder on sodium silicate-activated slag cement (AASC). Constr. Build. Mater. 292, 123257.
Zhu, X., Li, Q., Kang, X., Deng, J., Yang, K., 2021. Nano-structural change of C(N)–A–S–H gel in alkali-activated slag pastes subjected to wetting-drying cyclic sulphate attack. J. Chin. Ceram. Soc. 49, 2529–2537.
Zulhan, Z., Agustina, N., 2021. A novel utilization of ferronickel slag as a source of magnesium metal and ferroalloy production. J. Clean. Prod. 292, 125307.